Relaxation of slow highly charged ions hitting thin metallic foils

Z. D. Pešić,[1,*] Gy. Vikor,[1] S. Atanassova,[1] J. Anton,[1,†] S. Leontein,[2] M. Björkhage,[2] A. Paál,[2] H. Hanafy,[1,‡] and R. Schuch[1,§]

[1]*Atomic Physics, Fysikum, Stockholm University, AlbaNova, S-106 91 Stockholm, Sweden*

[2]*Manne Siegbahn Laboratory, S-104 05 Stockholm, Sweden*

(Received 7 July 2006; published 22 January 2007; publisher error corrected 23 January 2007)

We developed a method to determine the relaxation time of the innermost vacancies for highly ionized heavy ions moving through the bulk. The method compares the intensities of photons emitted through the front and back sides of a thin metal foil. Using foils with known thickness and x-ray absorption cross sections, we directly obtained the mean x-ray emission depth, and thereafter the mean relaxation time. We present data for the emission depth of highly charged $8.5q$ keV and $23.5q$ keV Pb^{q+} ions ($q=53-58$) impacting on thin Ta foils. The mean relaxation time of M-shell vacancies is estimated to be between 22 and 68 fs, depending on charge state of the projectile, which is about five times longer relaxation time than reported by Hattas *et al.* [Phys. Rev. Lett. **82**, 4795 (1999)]. The experimental results are supported by a model calculation that combines molecular-orbital calculation for the Pb^{54+}-Ta interaction system with a rate-equation model for inner-shell relaxation.

DOI: 10.1103/PhysRevA.75.012903 PACS number(s): 34.50.Dy, 32.30.Rj

I. INTRODUCTION

Studies of highly charged ion (HCI)-surface interaction [1], e.g., electron [2–4], x-ray [5,6] and energy-loss spectroscopy [7,8], and charge-state distributions of the scattered projectiles [9–11] have contributed to understanding the formation and stabilization of hollow atoms. This holds particularly for the first stage of hollow atom formation when a slow, highly charged ion is neutralized as electrons from the conduction band are transferred over a potential barrier into highly excited states of the ion. The hollow atom formation is described by the overbarrier model (OBM) [12] and experimentally verified by measuring the influence of the image-charge effect on the scattering angle [13]. Recent studies of the interaction of HCIs with metallic capillaries have revealed the stabilization of hollow atoms in vacuum [14,15].

According to the OBM, an ion with charge state $q=55$ captures the first electron at a distance about $d_c \approx 59$ a.u. above the surface, into a state with the principal quantum number $n \approx 49$. The complete neutralization occurs promptly as a large number of electrons (equal to the ion initial charge q) is captured into high Rydberg states. The subsequent relaxation by Auger cascading is not fast enough for the ion to be stabilized during the short approach time of a few femtoseconds before entering the bulk. Experiments in the early 1990s showed that the relaxation of the projectile occurs mainly below the surface [2,4]. For example, the Groningen group studied Auger electron spectra emitted in the interaction of 150 eV–20 keV N^{7+} with a Ni(110) metal monocrystal [4]. Sharp *KLL*-Auger peak at the low-energy side of the spectra was identified as above-surface emission while the majority of electrons are emitted below the surface and form broad peaks. Tuning the impact energy of the projectile (i.e., the above-surface relaxation time of the projectile) the ratio of the above-surface to the below-surface Auger-electron yield changes. In average, two electrons were found to be present in the L shell of the projectile when a K Auger electron is emitted above the surface, and five are present, if emission takes place below the surface.

Investigations based on Auger spectroscopy are limited to the above-surface and the near-jellium edge regions due to the energy loss of Auger electrons emitted inside the bulk (the mean free path is about 1 nm). Therefore, to investigate the relaxation of projectiles inside the bulk, the detection of x-rays is an alternative method. This is particularly the case for high-Z projectiles due to the increased fluorescence yield. Using x-ray crystal spectrometer, Briand and co-workers [6] resolved the K satellites that correspond to different numbers of L and M spectator electrons emitted in the interaction of 34 eV to 170 keV Ar^{17+} ions with a conducting surface. For low-impact energy (order of ~100 eV), the projectile K-shell vacancy is filled in the presence of a few L-shell electrons, while for much higher energy (few keV) interaction takes place mainly below the surface and L-shell filling is faster. For example, in the KL^x satellite spectrum (here, x represents the number of spectator electrons in the shell), lines with more spectator electrons are present ($5<x<8$) for high-projectile energy, while lines with larger number of vacancies ($1<x<3$) are dominant for the impact of projectiles with decreased impact energy. The mean time for one cascade is estimated to be in the order of $10^{-15}-10^{-16}$ s [6].

It has been proposed that the charge of the projectile is screened below the surface by a dynamic screening cloud

*Present address: Western Michigan University, Physics Department, Kalamazoo, MI 49008, USA and Advanced Light Source, Lawrence Berkeley National Laboratory, Berkeley, CA 94720, USA.

†Present address: Institut für Physik, Universität Kassel, D-34109 Kassel, Germany.

‡Permanent address: Beni-Suef Faculty of Science, Physics Department, Beni-Suef, Egypt.

§Corresponding author. Electronic address: schuch@physto.se

formed by conducting band electrons [16]. A calculation with density functional theory (DFT) shows that for Ne hollow atoms in aluminum, the screening cloud has the character of the M shell. Electrons that form the screening cloud might take part in the Auger relaxation process, i.e., the filling of the innermost vacancies might also occur by the KLC Auger transitions, where the screening cloud is denoted by C. Moreover, the internuclear distance between projectile and crystal atoms may become small enough to allow core electrons to be promoted into the L shell of Ne [16]. The process named side-feeding is an analogy to electron promotion [molecular orbital (MO)] in ion-atom collision [17]. Therefore, the inner-shell vacancies relax either by radiative and nonradiative transitions or by direct filling from the target atom's inner shells.

Beside fundamental aspects, the investigations of the interaction of HCI with solid surfaces are of genuine interest due to possible applications. It has already been prompted in the eighties that the high potential energy carried by HCIs might be exploited for surface modifications. For example, the use of potential sputtering for nanostructuring would avoid unwanted damage caused by using fast ions. Therefore, there is a quest for the exact time/depth scale for the energy deposition. On the other hand, there are very few direct experimental determinations of the relaxation time in the bulk [18–20]. One of the first estimates of the total relaxation time has been derived from the final charge state distribution of scattered ions (grazing angle collision of O^{q+} ions with Au(110) surface) [9]. These authors observed that charge-state equilibrium is reached within 30 fs that does not depend on the projectile charge state. The Livermore group reported a charge-state dependent energy loss of slow heavy ions transported through thin foils [19]. The results indicate a strong pre-equilibrium contribution to the energy loss of slow HCI in solids, and the upper limit for charge-state equilibrium of 21 fs is estimated. Later, the same group measured charge-state distributions of HCIs (0.5×10^6 to 1×10^6 m/s Xe^{33+} to Au^{68+}) transmitted through thin carbon foils [20]. The time to reach charge state equilibrium for Xe^{44+} and Au^{68+} ions is determined to be about 7 fs. However, the mechanism for such a fast equilibration is not known at present. Note that within 7 fs all inner-shell vacancies have to be filled, otherwise the charge state is going to increase after the projectile escapes from the foil, due to Auger transitions.

In the following, we study the relaxation dynamics of hollow atoms inside a solid using a method first described firstly in Ref. [21]. The method directly provides the depth in the bulk from where x-rays are emitted. Here, we detected M x-rays from Pb^{q+} ($53<q<58$) ions hitting Ta foils. The experimental results of the emission depth are combined with a trajectory simulation to obtain the slowing down of the ion in the solid, to get the range, and to convert the length scale to a time scale. We found that the relaxation time ranges from 30–60 fs. The obtained mean relaxation depths and times were verified for different experimental conditions (e.g., projectile velocity and thickness of the foil), where the slowing down (range) and absorption were varied and the experiments gave consistent results for the different parameters.

We used the relaxation model that was originally developed to explain above-surface neutralization [10] and combined it with a molecular orbital (MO) calculation for the Pb-Ta collision system for treating the relaxation of the projectile inside the bulk. The MO calculation gives the projectile levels that are filled in close collisions with target atoms, and from there the filling of inner atomic levels by radiative and nonradiative transitions is modeled by coupled rate equations. The calculated mean relaxation time is found to be in fair agreement with the experimental results. However, the relaxation model uses averaged transitions rates, and it is not sensitive enough to predict the charge-state dependence of the emission depth found in the experiment. We discuss possible processes responsible for the charge-state dependence of the emission depth and propose that Coster-Kronig transitions lead to a fast rearrangement of electrons within the shell whereby high-j sublevels are emptied, and therefore, the radiative rate gets reduced. Based on this argument, the charge-state dependence of the emission depth is obtained using a fitting procedure, where the lifetime of a single M-shell vacancy runs as a free parameter (see the Appendix).

II. EXPERIMENT

The experiment was performed at the Manne Siegbahn Laboratory in Stockholm. The highly charged ions, produced by an EBIS-type ion source named Cryogenic Stockholm Ion Source (CRYSIS) [22], were transported by an electrostatic lens system over a distance of 10 m to the interaction chamber. The charge state was selected by a dipole magnet, while the charge state of Pb^{52+} ions ($A=208$) was calibrated by He^+ ions that are used for ion cooling during confinement in the ion source. The vacuum in the beam line was 2×10^{-8} mbar. The pressure in the interaction chamber (flight path around 30 cm) was in the upper 10^{-8} mbar range. Therefore, the electron-capture probability from the rest gas was low. The beam was collimated by a set of apertures onto the target; one circular of 8 mm diameter and one ellipsoid aperture (axis lengths 4 and 9 mm; the longer axis was oriented parallel to a target holder). The last aperture was positioned 2 cm away from the target to screen the target holder from being directly hit by ions. Both the apertures and targets were isolated from the ground in order to monitor the beam stability and the ion current on the target. Ratios of the ion current measured at different checkpoints along the ion flight path were kept constant during the run, and the fluctuations of the beam current were normalized. The collected charge per pulse was typically 4 pC, the pulse was stretched up to 80 ms in order to avoid the pulse pileup in the signal processing from the Si(Li) detectors. Perpendicular to the incident beam direction two Si(Li) detectors (see Fig. 1), with energy resolution 170 and 180 eV at 5.9 keV, were positioned. The energy scales of the detectors were calibrated using a ^{55}Fe source that gives Mn (5.9 keV and 6.5 keV) K x-ray lines, and by fluorescence lines of Ti (4.5 keV) and Si (1.7 keV).

The target holder was mounted on a standard manipulator with 4° of freedom and oriented 450 relative to the ion-beam direction, which allowed simultaneous detection of photons

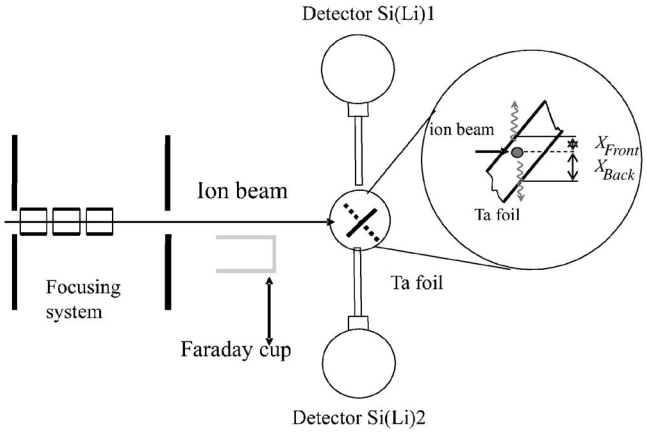

FIG. 1. The schematics of the experimental setup (not to scale). Two Si(Li) detectors used in the present experiment are labeled as Si(Li)1 and Si(Li)2.

that escape through the back and the front surfaces of the foil. In the following, we name the spectra that are related to these two different target orientations *back side* and *front side*. So we obtained two sets of spectra from Si(Li)1 and Si(Li)2 (see Fig. 1). During the measurement, we changed the detection geometry by rotating the target back and forth 900 every 2 h [changes the Si(Li) detectors *view* between back side and front side of the foil], and the normalized spectra were averaged over independent runs for the particular impact energy and initial charge.

The foil material was carefully selected to accomplish a high photon-absorption cross section in the expected range of x-ray energies, to avoid characteristic fluorescent lines and to stop the projectile entirely. One target position remained empty in order to check possible contributions of x-rays from ions hitting the target frame. This contribution was found to be less than 2%.

The accurate value of the foil thickness is crucial for the data analysis. It was determined by using Rutherford backscattering (RBS) of 1.5 MeV protons and 2 MeV He^+ ions. Five independent runs were made for each foil (three runs with a proton beam and two runs with a He^+ beam). The foil thicknesses were determined using both the height (normalized intensity) and the width [full width at half maximum, (FWHM)] of the RBS spectra [23]. The thicknesses of the foils used in the experiment were then calculated as the mean value of the ten independent results (five from the height and five from the width of the RBS spectra). The thick Ta foil (456±6 nm, in a sample holder with 9 mm diameter hole) was self-supporting, while the thin Ta foil (65±1 nm, 9 mm diameter) was evaporated on a carbon support (90 nm).

In order to be able to determine the mean emission depth, the projectile needs to be stopped inside the foil. It was therefore important to estimate the range of the ions. The penetration depth of Pb^+ ions in the bulk was calculated by the SRIM2000 program [24] (the 2000 version of commonly used TRIM code [25]) for impact energies ($8.5q$ keV, $53 < q < 58$). An upper limit for the mean penetration depth of the Pb^{q+} ions is found to be 40 nm.

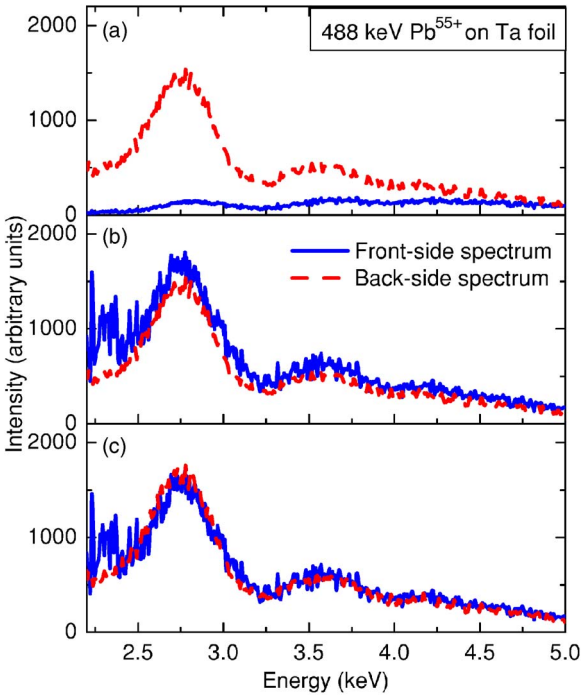

FIG. 2. (Color online) Front-side (solid line) and back-side (dotted line) x-ray spectra from the interaction of Pb^{55+} ions with a Ta foil. Front and back sides are named according to the ion-beam direction. (a) The spectra are corrected for the absorption in detector's Be window and Si crystal; (b) back-side spectrum is corrected for the absorption of the full Ta thickness; (c) the spectra are corrected for appropriate photon path to achieve the best agreement.

III. ANALYSIS OF THE X-RAY SPECTRA

The difference of the intensity of front- and back-side x-ray spectra is caused by different path lengths through the absorbing material (Ta foil) as well as by different detection efficiencies of the two Si(Li) detectors. Therefore, we introduced two normalization functions. The *geometrical function* takes into account the solid angle of the detectors. Both detector solid angles (estimated initially from the geometry of the setup) were about 0.12 sr. The data analysis showed that the left Si(Li) detector was in fact closer to the target than the right one by about 8%, giving a somewhat different geometrical factor. The second normalization factor, named *photon-energy-dependent* function corrects for the detection efficiency of the detectors and for the photon absorption by the target. Here, the target includes the target foil material and beryllium window of the detector.

The data were first normalized using the high-energy parts of the photon spectra (between 4 and 5 keV photon energy), where the correction by the photon-energy-dependent function is reduced (photon attenuation is between 20% and 10% of the value at 2 keV). The obtained geometrical factor was thereafter used to determine the photon-energy-dependent function. These iterations were repeated until the corrections were negligible. The convergence was very strong; only a few steps were needed. The influence of the background radiation was also taken into account and the experimental spectra were corrected.

The normalization procedure is illustrated in Fig. 2 where x-ray spectra emitted from the interaction of $E=8.5q$ keV Pb^{55+} ions with a tantalum foil of 65 nm thickness are plotted. In Fig. 2(a) spectra of x-rays emitted through the front side (solid line) and back side (dotted line) of the target foil are shown. The correction for the absorption by the detector's Be window (25 μm), the dead layer of the Si crystal (0.1 μm), and the Au contact (100 Å) is made for both spectra. Additionally, the back-side spectrum is corrected for the absorption by the carbon support of the Ta foil. So far, no correction is done for the absorption by the Ta. In Fig. 2(b), the back-side spectrum is corrected for the absorption by the full thickness of the Ta foil, i.e., it is assumed that the x-rays are emitted when the ions are still above the surface. The poor overlap of front- and back-side spectra [see Fig. 2(b)] clearly shows that it is necessary to correct both spectra for the proper absorption by the Ta foil.

The fitting procedure where the emission depth runs as a free parameter results in overlapping front- and back-side spectra. Figure 2(c) shows both spectra after the absorption correction for the emission depth. The front-side spectrum (solid line) is corrected by the calculated depth d_{em}, while the back-side spectrum (dotted line) is corrected for the absorption by the remaining part of the target thickness $(d_{foil}-d_{em})$. The same data analysis was carried through for both thicknesses of the target foil (65 nm and 456 nm), for both ion energies (8.5q keV and 23.5q keV) and for all projectile charge states $(53<q<58)$. Values of the emission depth obtained in independent runs were averaged.

In the error analysis, the influence of uncertainties in the various contributions on the accuracy of the measured emission depth was estimated. First of all, the roughness of foils was checked by means of secondary electron microscopy (SEM). We found that for the thicker Ta foil (456 nm) it was below 0.5%, while the thinner one (65 nm) showed relatively higher roughness, about 5%, where the periodicity of these "waves" is in the order of micrometers. We argue that the experimental results are not influenced by these roughnesses, i.e., they are "smoothed" as the size of the ion beam was few millimeters. Second, the pileup of detected x-ray signals was kept to a percent level by stretching out the duration time of the bunch of the projectile beam. Finally, backscattered ions can influence the value of the emission depth as x-rays could be emitted above the surface and increase the yield of the front-side spectra. From SRIM calculation we find that for 500 keV Pb impact under 450, 5% of ions are backscattered, which is a negligible amount.

IV. RESULTS AND DISCUSSION

This chapter is organized in the following way. The experimentally determined mean emission depths and corresponding mean relaxation times are presented in Sec. IV A. The theoretical modeling consists of two parts: the molecular-orbital (MO) quantum mechanical calculations (presented in Sec. IV B) give possible capture channels. These are fed into the rate equation model for inner-shell relaxation (Sec. IV C). The model calculation reproduces the mean relaxation time, but not the charge-state dependence of the relaxation time seen in the experiment. In the following, we discuss possible reasons that the model calculation reproduces the mean relaxation time but not the charge-state dependence of the relaxation time, and we also give a comparison with previous results for the relaxation time [20]. In the Appendix, we explain how the relaxation of the projectile is analyzed for different charge states and the relaxation time for M-shell vacancies is estimated. The charge-state dependence of the mean relaxation time is reproduced by this fitting procedure.

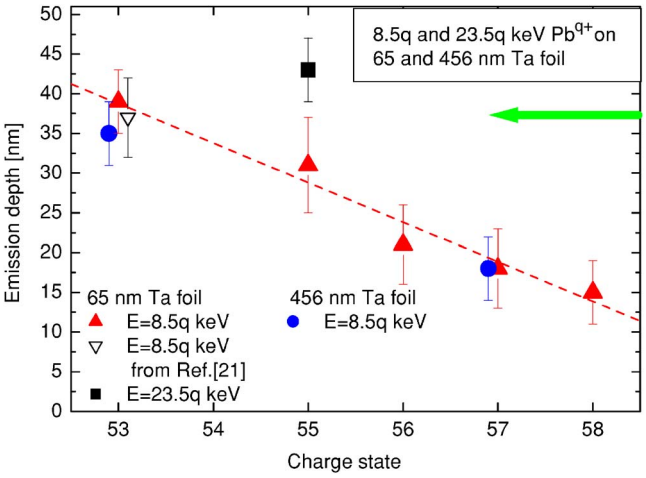

FIG. 3. (Color online) Emission depth for 8.5q keV Pb^{q+} $(53<q<58)$ ions impinging on Ta foils (thicknesses were 65±1 nm and 456±6 nm). The mean ion range obtained using SRIM2000 code is presented as a horizontal arrow. The line is drawn to guide the eye.

A. Mean emission depths and relaxation times

Figure 3 shows the dependence of the emission depth on the projectile charge state, varied from $q=53$ to $q=58$ for an energy of 8.5q keV. The data are presented for tantalum foils with thicknesses of 65±1 nm and 456±6 nm. The mean emission depths are determined as a weighted average of a large number of independent runs, using the normalization procedure described in Chapter 3. The results are arranged in Fig. 3 and Table I. The value published previously [21] for 8.5 keV Pb^{53+} projectiles is also presented, and is found consistent with the present data.

The mean ion range obtained using the SRIM2000 code is presented as a horizontal arrow. The mean ranges increase slightly from 37±18 nm for Pb^{53+} ions to 40±19 nm for Pb^{58+} ions, due to an increase in the impact energy. The range of 23.5q keV Pb^{55+} ions is found to be 93±42 nm (not plotted in Fig. 3). These trajectory simulations indicate that the projectiles still move when the M x-rays are emitted.

The reliability of the applied technique is demonstrated by the good agreement found for the emission depths for thin (65 nm) and thick (456 nm) foils (500 keV Pb^{55+} ions). It should be noted, that for different energies of the projectile (e.g., for Pb^{55+} with energy 8.5q keV and 23.5q keV), the projectile emission depths are different. However, the mean relaxation time is the same (as shown later), although the

TABLE I. Emission depth as a function of the projectile charge state. The data are presented for Ta foils with thicknesses 65 nm and 456 nm as well for two impact energies.

Pb^{q+}	Emission depth (nm)		
Charge state	Thin target (65 nm)		Thick target (456 nm)
(q)	$E=8.5q$ (keV)	$E=23.5q$ (keV)	$8.5q$ (keV)
53	39±4		39±4
55	31±6	43±4	
56	21±5		
57	18±5		18±4
58	15±4		

emission depth increases by about 50%, going from $8.5q$ keV to $23.5q$ keV.

Note that M x-rays are emitted even for Pb^{53+} projectiles, which do not have initial M-shell vacancies. The mechanism for vacancy creation in Pb^{53+} via internal dielectronic excitation (IDE) according to Refs. [21,26] is as follows: doubly excited states, such as $3d^9 4141'$ are energetically degenerated with singly excited states $3d^{10}nl'$ ($n \geqslant 8$) and this opens up the M shell. The M vacancy may then decay as M x-ray. IDE thus provides a channel for fast transfer of electrons from high-Rydberg states $3d^{10}nl'$ ($n \geqslant 8$) to the N-shell ($3d^9 4141'$); therefore, the emission of M x-rays could occur promptly and near the surface. Indeed, it has been reported that photons emitted due to the IDE are emitted above the surface [27]. More insights into these processes for Pb^{q+} studied by means of coincident photon detection will be published elsewhere [28].

The most striking result is that the emission depth shows a counterintuitive charge-state dependence, i.e., the emission depth decreases for increasing charge state of the projectile. The measured values represent the emission depths averaged over the depth of all emitted photons. It is clear that ions with higher charge state (e.g., Pb^{58+}) need more time to relax completely. Therefore, it appears that the presence of more M-shell vacancies speed up the relaxation and the first M x-rays are emitted earlier than for the projectiles with lower charge state ($q<58$). The charge-state dependence of the emission depth is discussed in details in the following sections and in the Appendix.

The experimentally determined mean emission depths have been used in combination with classical trajectory calculation SRIM2000 to determine the time scale for the relaxation. We followed a large number of projectile trajectories through the solid (10 000 for each of projectile impact energy), recording the coordinates and the energy of the projectiles for every collision with target atoms. The time scale for relaxation has been extracted by gating the numerical output of the simulation by the experimentally determined mean relaxation depth. The mean relaxation times for Pb^{q+} ($q=53,55,58$) with energy $8.5q$ keV and $23.5q$ keV are presented in Table II. Similar to the charge-state dependence of the mean emission depth, the mean emission time also decreases with increasing the number of vacancies in the M shell. It reads from 22 fs for Pb^{58+} up to 68 fs for Pb^{53+} ions. For the case of Pb^{53+} ions, the relaxation depth is close to the mean ion range and the presented relaxation time is a lower limit, as photons can be emitted when the ions are coming to a stop. Note that the mean relaxation time (within the error bars) is the same for both impact energies ($8.5q$ keV and $23.5q$ keV) of Pb^{55+} projectile. The mean emission depth is about 50% higher for $23.5q$ keV Pb^{55+} than for $8.5q$ keV Pb^{55+}, but the time scale for the relaxation remains the same.

B. Molecular orbital calculation

As explained in the Introduction, the filling of projectile levels when it enters the bulk is effectuated by "side feeding," which can be treated by coupling between molecular orbitals (MOs). In order to find the levels for direct filling of inner projectile shells, we performed MO calculations for the Pb-Ta collision system. The computational details of this method are presented elsewhere [29,30], thus only a short description is given here. The calculation was performed for 500 keV Pb^{54+} scattered on a Ta atom where the Bohr potential was used to calculate classical trajectory of the nuclei. The electron dynamics is determined by a time-dependent Hamiltonian. The wave function of the whole system is a Slater determinant built from time-dependent single-particle wave functions. The latter ones are expanded in a set of static molecular orbital basis functions, which are only implicitly time dependent. The explicit time dependence is contained in the expansion coefficients (single-particle amplitudes). The basis functions are a solution of the static Dirac-Fock-Slater (SDFS) equation. It has been solved self-consistently for 90 internuclear distances using the MO-LCAO (molecular orbital linear combination of atomic orbitals) method, providing single-particle energies. For every internuclear distance,

TABLE II. Relaxation time determined for ions with different charge state and incoming energy.

Pb^{q+}	Relaxation time (fs)	
Charge state (q)	Energy$=8.5q$ (keV)	Energy$=23.5q$ (keV)
53	68±10	
55	50±8	42±4
56	35±6	
57	30±5	
58	22±4	

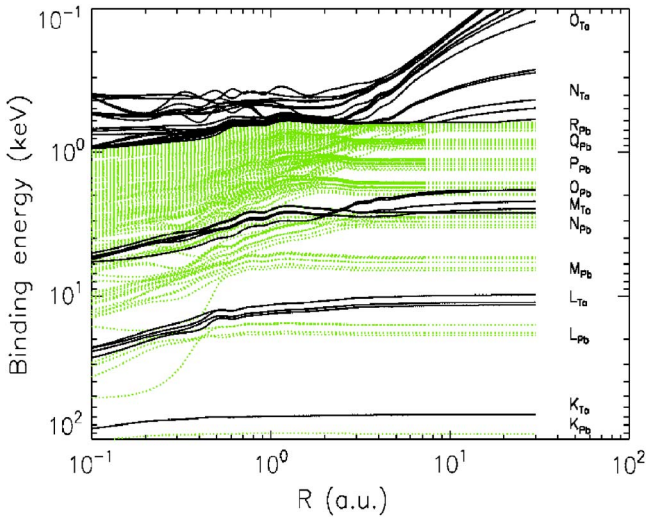

FIG. 4. (Color online) Correlation diagram for Pb^{54+}-Ta system. Initial tantalum levels are plotted as solid lines, while initial Pb levels are plotted as dashed lines.

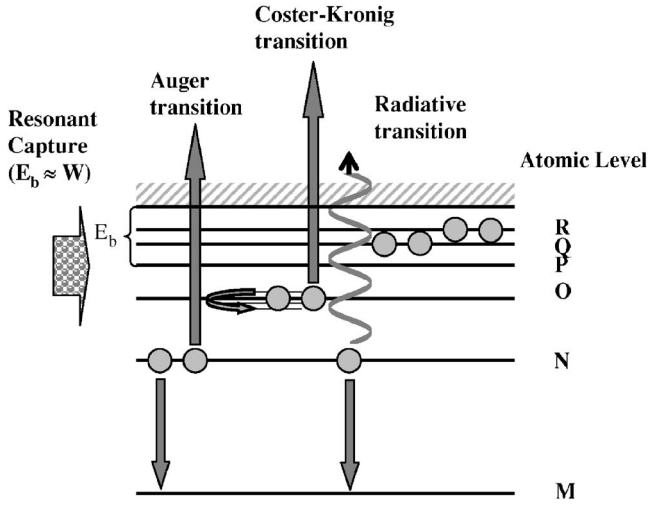

FIG. 5. Schematics of the processes included in the relaxation model.

electrons are distributed into molecular states that correspond to the asymptotical atomic ground states of the Ta atom and Pb^{54+} ion (transition state population). We neglected electrons captured during approach to the surface. Using calculated single-particle energies and the dynamic coupling matrix elements, the close-coupling equations were solved. According to the molecular orbital calculations, a direct filling of the Q and R shells ($n=7,8$) of Pb is possible at about 3 a.u. (see correlation diagram in Fig. 4). At internuclear distances below 2 a.u., even a direct filling of the N shell of Pb could take place. However, the N-shell filling has a low probability in comparison to the filling of Q and R shells.

Note that the MO calculation provides a starting configuration for the rate equation model. Further influences of the solid environment are neglected. Thus Q and R levels can be considered having the contribution of both bound and continuum states [31].

C. Rate-equation model for inner-shell relaxation

The relaxation of the Pb ions inside the bulk is modeled using rate equations. The model has been developed originally for above-surface neutralization of highly charged ions [10]. It considers resonant filling (side feeding) of projectile shells and their reionization by Auger transitions. The processes included in the model are shown schematically in Fig. 5. To simulate the below-surface relaxation, several modifications of the original code have been made. First, the model assumes that HCI will be promptly screened while entering the bulk, according to the description of a dynamic screening cloud [16]. Second, we use the result of the MO calculation (instead of side feeding) as an input for the rate equations and initially populate Pb levels with principal quantum numbers $n=7$ and $n=8$ equally with electrons. The model predictions have also been tested for nonequal distributions of electrons in these levels, but no significant dependence on the initial configuration has been found. The relaxation occurs mainly by nonradiative transitions. Radiative transitions are considered only for the M shell. The model presumes that the projectile remains neutral within the bulk, and the electrons ejected due to the Auger and Koster-Cronig processes are replaced by captured ones. These electrons are, at the beginning, distributed into $n=7$ and 8 levels. Note that direct filling of lower levels of the projectiles can occur in a later stage of relaxation when the projectile electron states are shifted upward in energy due to the screening by already transferred electrons and might come into resonance at states near the Fermi edge. We allow for electron capture to lower levels than $n=7$ and $n=8$, under the condition that the binding energy of the electron is in resonance with the conduction band. Hydrogenlike levels were assumed by $E_n \propto Z_{eff}^2/2n^2$, where Z_{eff} has been calculated using Slater's rules for screening [32].

Most of the Auger transition rates for multiply excited ions are unknown, thus a semiempirical scaling law has been used. The Auger rate of multiply excited states Γ^{ijk} is set to be proportional to the number of vacancies n_v^i in the lowest transition level i and product of square roots of the number of electrons in the levels j and k (n_e^j and n_e^k, respectively), i.e., $\Gamma^{ijk} \propto \Gamma_o^{ijk} n_v^i \sqrt{n_e^j} \sqrt{n_e^k}$. A similar correction for the number of equivalent electrons has been used by many authors [7,10,12,16]. The value Γ_o^{ijk}, i.e., Auger transition rate per spin state is scaled as proposed by $\Gamma_o^{ijk} = \Gamma_o / \Delta n^{3.46}$ in Ref. [12], where Δn is the difference of principal quantum numbers and Γ_o is the adjustable parameter. When the involved electrons are not in the same shell, the rate decreases by a factor of 3 or 9, depending upon whether the electron's principal quantum number differs by 1 or 2, respectively. Radiative rates, as well as Coster-Kronig rates, were verified in Refs. [33,34]. A similar scaling law that accounts for the number of active electrons, has been applied for these rates ($\Gamma_x^{j \to i} \propto \Gamma_o^{ij} n_v^i n_e^j$ and $\Gamma_{CK}^{ijj} \propto \Gamma_{CKo}^{ijj} n_v^i n_e^j$).

The fitting parameters Γ_o, Γ_o^{ijj}, and Γ_{CKo}^{ijj} are adjusted to reproduce the experimentally obtained ratio of the intensities $M_\alpha / M_\beta = 1.4 \pm 0.2$. By setting $\Gamma_o = 2 \times 10^{12}$, typical Auger rates are in the range $10^{14}-10^{15}$ s^{-1}, which is reasonable ac-

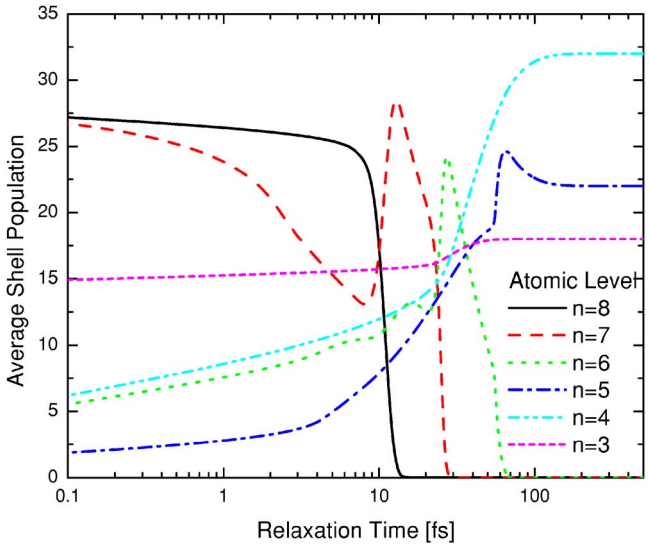

FIG. 6. (Color online) Time evolution of the shell populations of Pb^{58+} ion inside the bulk.

cording to a recent calculation [35]. The used Coster-Kronig rates are one order of magnitude faster than the Auger rates. To activate a certain Coster-Kronig channel, e.g., *NNO*, the binding energy of the *O*-shell electron is compared with the separation of the *j* sublevels of the *N* shell, where the energy of levels and sublevels with different angular momentum is calculated assuming a hydrogenlike structure.

The time evolution of the shell population and mean relaxation time $\bar{\tau}=(\int Y_{\alpha+\beta}(t)tdt)/(\int Y_{\alpha+\beta}(t)dt)$ is determined by numerically solving the system of coupled differential equations [10], where $Y_{\alpha+\beta}$ represents the time-dependent x-ray yield. The time evolution of shell populations is presented in Fig. 6 for Pb^{58+} ion. This charge state $q=58$ has been chosen to minimize the effect of the creation of extra vacancies by the IDE process. Figure 6 indicates that the initial highly excited population decays to the ground state within 20–50 fs and the mean relaxation time is found to be 25 ± 6 fs. This is in agreement with the relaxation time of 22 fs from the experiment. It is interesting that the model predicts that the emission of M_β x-rays starts earlier than the emission of M_α x-rays, as soon as the first electron is transferred into the *O* shell, and dominates for some time over to M_α emission. Later, the number of electrons in the $n=4$ level exceeds the number of electrons in the $n=5$ level, producing finally $M_\alpha/M_\beta=1.4$. This value $(M_\alpha/M_\beta=1.4\pm0.2)$ is about five times larger than the value obtained by Chen and Crasemann [36] for atomic Pb. The ratio of their values for $A^\alpha{}_o=1.5\times10^{13}$ s^{-1} and $A^\beta{}_o=0.2\pm10^{13}$ s^{-1} is 7.5 which indicates that a large number of electrons in *O* shell is present when the photons are emitted. The model predicts the fluorescence yield of 3%, which is in agreement with the experiment [28] and this justifies the transition rates used in the calculation.

The rate-equation model is not able to reproduce the measured charge-state dependence of the mean relaxation depth. The x-ray rates were scaled with the product $Y_{\alpha+\beta}(t)\sim n_{3v}(t)n_{4,5e}(t)$ and this product is higher for the projectiles with the higher charge state, but the *gravity* of $Y_{\alpha+\beta}(t)$ is not time shifted. We considered processes that might *speed up N*- and *O*-shell filling for the ions of highest charge states used here. We ruled out orbital crossings as a possible reason. Also, the creation of an additional vacancy by IDE happens in an early phase of the relaxation where high-Rydberg levels are populated [21], and more important, it occurs also for ions with initial *M*-shell vacancies [27,28].

The model does not account for different transition rates (Auger, Coster-Kronig, radiative) of subshells. The typical transition rates ordered according to the magnitude are from 10^{15}–10^{16} s^{-1} for the fastest Coster-Kronig, down to 10^{14}–10^{15} s^{-1} for Auger and 10^{13} s^{-1} for radiative transitions. It is clear that Coster-Kronig transitions, which are one to three orders of magnitude faster than Auger and radiative transitions, will lead to the fast intrashell rearrangement. Thus electrons in the high *j* subshells will be depleted rapidly. On the other hand, for Pb with vacancies in the 3*d* subshell faster radiative transitions are in fact 4*f*-3*d* and 5*f*-3*d*. For example, the probability for an M_5-subshell vacancy filling by a radiative transition that leaves the final vacancy in N_6 and N_7 subshells is three orders of magnitude larger than the probability for the transition where the final vacancy is produced in the N_1 or N_2 subshell. Therefore, the charge-state dependence of the relaxation depth can be explained by taking into account a competition between Coster-Kronig and radiative transitions. The Pb^{58+} projectile has four vacancies in the 3*d* subshell and the x-ray yield is significantly higher than for projectiles with charge state $q<58$ used here. An enhancement of $Y_{\alpha+\beta}(t)$ distribution for ions with increased number of *M*-shell vacancies thus exists in the beginning of the relaxation process, i.e., at the moment when the first electrons are transferred into *N* and *O* shells. As soon as Coster-Kronig transitions become energetically allowed, mainly low *j* subshells remain populated and the average x-ray yield decreases by an order of magnitude. Thus, the large numbers of photons for Pb^{58+} projectile are emitted at the very beginning, when Coster-Kronig transitions are still forbidden.

The multiplicity of involved transitions for different *j* levels would make a model calculation very complex. That is the reason why we considered shell average rates. The relaxation of the projectile was analyzed for different projectile charge states in the Appendix. We calculated the emission depths as a function of the charge state of the projectile (related to the number of vacancies *n*), where we used the lifetime of an *M*-shell hole as a free parameter. The results from the fits are presented in Fig. 7. The slope of the fitted line is directly proportional to the lifetime of the *M*-shell hole in the bulk. Note that one extra vacancy is added in the *M* shell (see Refs. [21,26–28]) for all initial charge states to include the IDE process. The model fit of the experimentally determined multiple photon emission (the integrated relaxation time of 30 fs to 60 fs) gives the relaxation time of a single *M*-shell hole of 30–60 fs. The emission depth and the corresponding integrated relaxation time show the measured charge-state dependence (Fig. 7).

The present values for the relaxation time are three to six times longer than those published in Ref. [20], where it is stated that highly charged ions reach the equilibrium charge within less than 10 fs. Using the isolated atomic Auger and radiative rates, the total relaxation time would be much

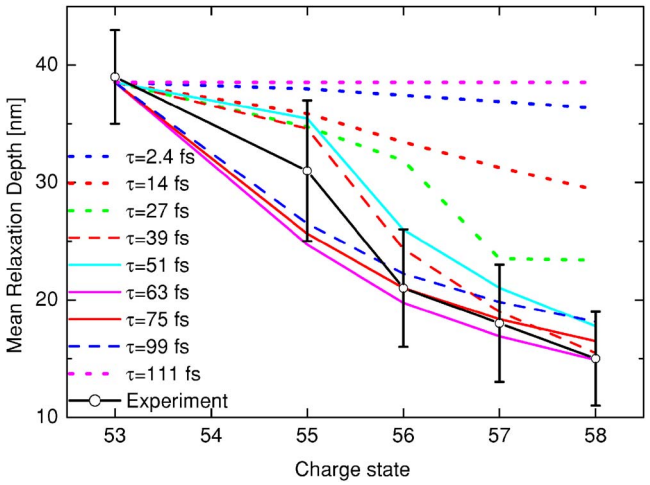

FIG. 7. (Color online) *M*-shell vacancy lifetime as a function of the initial number of *M* vacancies. The model fit shows that with increasing number of *M* vacancies, the mean lifetime is decreasing, with the same tendency as seen in the experiment.

longer (order of ps). The time to reach the equilibrium charge cannot be shorter than the mean relaxation time of the *M*-shell vacancy, as the *M*-shell vacancy relaxation by Auger transition creates a hole in the upper shell. Hattas *et al.* [20] estimated that the screening cloud is formed after a few fs and that for Au^{68+} ion at least ~100 transitions have to take place within 7 fs. The typical Auger transition rates of 10^{15} s^{-1} are too slow for getting 100 transitions in 5 fs. It has therefore been suggested that multiple-transition cascades proceed [20].

In spite of the difference in relaxation times, we think it may be possible to explain the result of both experiments by a common model for the relaxation. The different projectile-target combinations (Au^{q+}-C and Pb^{q+}-Ta) and different experimental situations (ions transmitted through the foil and ions stopped in the bulk) need to be taken into account. First, higher *n*-levels are initially populated in the Pb^{q+}-Ta interaction as compared to the Au^{68+}-C foil interaction ($n=5-6$); therefore, more steps are necessary to populate the inner shell. Additionally, in the present case, the complete relaxation occurs in the bulk, while Hattas *et al.* measured the charge-state distribution of ions transmitted through the foil [20]. On the trajectory after the ion escapes from the solid, relaxation can occur mainly by radiative transitions, which would make the time to appear shorter as there is no increase of the final charge state.

V. CONCLUSION

We measured the depth where HCIs relax by x-ray emission inside solids. We found a mean emission depth of typically 50 to 100 atomic layers inside the bulk and a significant decrease of nearly a factor of 3 of the depth with increasing the charge state of the projectile. The experimental results for the emission depth were combined with classical trajectory calculations for getting a mean filling times of *M*-shell vacancies, which is a measure for the relaxation time of the hollow atom inside the bulk. Values reaching from 22 fs for Pb^{58+} projectiles up to 68 fs for Pb^{53+} projectiles were obtained, which are much longer than previously determined by a different method for a different system [20].

We interpreted the results by a two-step relaxation-dynamics model. MO calculations provide initial configurations for the hollow atoms in the bulk. The decay is then simulated by a rate-equation model. This results in a mean relaxation time that is in agreement with the experimental value. On the other hand, the charge-state dependence of the relaxation time cannot be explained by the rate-equation model. We propose that higher x-ray yields for projectiles with increasing *q* occur when *N* and *O* shells are populated with very few electrons and the Coster-Kronig transitions do not play a significant role. Additionally, a multiple emission of photons is fitted using the analytical equation and a mean decay time of the single *M*-shell vacancy is obtained to be about 40 fs.

ACKNOWLEDGMENTS

We appreciate the beam time for the Rutherford backscattering measurement, provided by the group of B. Emoth, Royal Institute of Technology (KTH), Kista, Sweden. We gratefully acknowledge the financial support from the Swedish Research Council (VR) and one of the authors (J.A.) from the Deutsche Forschungsgemeinschaft (DFG).

APPENDIX: RELAXATION TIME FOR A SINGLE *M*-SHELL VACANCY

The emission-depth decrease with increasing projectile charge state seems counterintuitive, as it should take a projectile with a higher charge state longer depth/time within the bulk to relax. There is, however, the consideration of the sequential radiative decay of inner-shell vacancies on the path and the difference in the absorption of the photons on the way out of the bulk.

We start with ions with only one *M* hole. The measured *M* x-ray intensity is then related in the following way to all photons emitted by the ions, attenuated by the target absorption [21]:

$$I_{f/b} = I_o e^{-\sigma_m x_{f/X_b}} \Delta\Omega_{f/b}(E), \tag{1}$$

where I_o is the initial x-ray intensity, σ_m absorption cross section, $x_{f/b}$ average emission depth, and $\Delta\Omega_{f/b}(E)$ are the solid angles of x-ray detectors at the front and back sides of the foil. Here, $x_f+x_b=D$ is the thickness of the target foil.

If an ion has $n>1$ *M*-shell holes, then it can emit up to *n* x-ray photons, which will be emitted sequentially in time, i.e., along the ion path at different $x_{f/b}$ and the front- and back-side intensities are

$$I_{f/b} = \sum_{k=1}^{n} I_o^k e^{-\sigma_m x_{f/b}^k} \Delta\Omega_{f/b}^k(E). \tag{2}$$

If the *k*th photon is emitted with the delay of τ_k after the first one, then the ion moves $\Delta X^k = \int_0^{\tau_k} v_x(t)dt$ and the emission depths can be written in the form $x_f^k = x_f^1 + \Delta X^k$ and $x_b^k = x_b^1 - \Delta X^k$.

Insertion of $x_{f/b}^k$ into Eq. (2) gives

$$I_{f/b} = e^{-\sigma_m x^1_{f/b}} \sum_{k=1}^{n} I_0^k e^{-2\sigma_m \Delta X_k} \Delta\Omega^k_{f/b}(E). \quad (3)$$

The last equation has been solved analytically to find the depth where the first hole is being filled,

$$x_f^1 = \frac{D}{2} - \frac{1}{2\sigma_m} \ln(I_f/I_b) + \frac{1}{2\sigma_m} \ln\left(\frac{\sum_{k=1}^{n} I_0^k e^{-\sigma_m \Delta X^k} \Delta\Omega_f^k(E)}{\sum_{k=1}^{n} I_0^k e^{\sigma_m \Delta X^k} \Delta\Omega_b^k(E)} \right). \quad (4)$$

In order to compare this formula to the experimental data, we made two assumptions: (i) all ions are uniformly decelerated through the bulk where the deceleration a_x was calculated from a mean penetration depth L (obtained by the SRIM program) as $a_x = E_i/ML$ (here M and E_i are the projectile mass and ion energy, respectively); and (ii) the mean fluorescence yield can be included in the M-hole lifetime and this does not depend on the initial number of M-shell vacancies. The later approximation is very rough, but it is chosen to make a simple estimate of the relaxation time, based on the measured data. The result of the model fit is presented in Fig. 7.

[1] A. Arnau, F. Aumayr, P. M. Echenique, M. Grether, W. Heiland, J. Limburg, R. Morgenstern, P. Roncin, S. Schippers, R. Schuch, N. Stolterfoht, P. Varga, T. J. M. Zouros, and H-P. Winter, Surf. Sci. Rep. **27**, 113 (1997), and references therein.

[2] F. W. Meyer, S. H. Overbury, C. C. Havener, P. A. Zeijlmans van Emmichoven, and D. M. Zehner, Phys. Rev. Lett. **67**, 723 (1991); F. W. Meyer, S. H. Overbury, C. C. Havener, P. A. Zeijlmans van Emmichoven, J. Burgdörfer, and D. M. Zehner, Phys. Rev. A **44**, 7214 (1991).

[3] F. Aumayr, H. Kurz, D. Schneider, M. A. Briere, J. W. McDonald, C. E. Cunningham, and H-P. Winter, Phys. Rev. Lett. **71**, 1943 (1993); H. Kurz, F. Aumayr, H-P. Winter, D. Schneider, M. A. Briere, and J. W. McDonald, Phys. Rev. A **49**, 4693 (1994).

[4] L. Folkers and R. Morgernstern, Europhys. Lett. **13**, 377 (1990); J. Das, L. Folkerts, and R. Morgenstern, Phys. Rev. A **45**, 4669 (1992); J. Das and R. Morgenstern, *ibid.* **47**, R755 (1993).

[5] E. D. Donets, Nucl. Instrum. Methods Phys. Res. B **9**, 522 (1985).

[6] J. P. Briand, L. de Billy, P. Charles, S. Essabaa, P. Briand, R. Geller, J. P. Desclaux, S. Bliman, and C. Ristori, Phys. Rev. Lett. **65**, 159 (1990); B. d'Etat, J. P. Briand, G. Ban, L. de Billy, J. P. Desclaux, and P. Briand, Phys. Rev. A **48**, 1098 (1993); J. P. Briand, G. Giardino, G. Borsoni, M. Froment, M. Eddrief, C. Sébenne, S. Bardin, D. Schneider, J. Jin, H. Khemliche, Z. Xie, and M. Prior, *ibid.* **54**, 4136 (1996).

[7] S. Winecki, C. L. Cocke, D. Fry, and M. P. Stöckli, Phys. Rev. A **A53**, 4228 (1996).

[8] W. Huang, H. Lebius, R. Schuch, M. Grether, and N. Stolterfoht, Phys. Rev. A **58**, 2962 (1998); R. Schuch, W. Huang, H. Lebius, Z. Pešić, N. Stolterfoht, and G. Víkor, Nucl. Instrum. Methods Phys. Res. B **157**, 309 (1999); Z. D. Pešić, J. Anton, J. H. Bremer, V. Hoffmann, N. Stolterfoht, Gy. Víkor, and R. Schuch, *ibid.* **203**, 96 (2003).

[9] L. Folkerts, S. Schippers, D. M. Zehner, and F. W. Meyer, Phys. Rev. Lett. **74**, 2204 (1995).

[10] W. Huang, H. Lebius, R. Schuch, M. Grether, and N. Stolterfoht, Phys. Rev. A **56**, 3777 (1997); Z. D. Pešić, H. Lebius, R. Schuch, Gy. Víkor, V. Hoffman, D. Niemann, and N. Stolterfoht, Nucl. Instrum. Methods Phys. Res. B **165**, 511 (2000).

[11] V. A. Morozov and F. W. Meyer, Phys. Rev. Lett. **86**, 736 (2001).

[12] J. Burgdorfer, P. Lerner, and F. W. Meyer, Phys. Rev. A **44**, 5674 (1991).

[13] H. Winter, D. Auth, R. Schuch, and E. Beebe, Phys. Rev. Lett. **71**, 1939 (1993).

[14] S. Ninomiya, Y. Yamazaki, F. Koike, H. Masuda, T. Azuma, K. Komaki, K. Kuroki, and M. Sekiguchi, Phys. Rev. Lett. **78**, 4557 (1997).

[15] K. Tökési, L. Wirtz, C. Lemell, and J. Burgdörfer, Phys. Rev. A **61**, 020901 (2000).

[16] M. Grether, A. Spieler, R. Köhrbrück, and N. Stolterfoht, Phys. Rev. A **52**, 426 (1995); N. Stolterfoht, A. Arnau, M. Grether, R. Köhrbrück, A. Spieler, R. Page, A. Saal, J. Thomaschewski, and J. Bleck-Neuhaus, *ibid.* **52**, 445 (1995).

[17] K. J. Snowdon, C. C. Havener, F. W. Meyer, S. H. Overbury, D. M. Zehner, and W. Heiland, Phys. Rev. A **38**, 2294 (1988).

[18] R. Herrmann, C. L. Cocke, J. Ullrich, S. Hagmann, M. Stoeckli, and H. Schmidt-Boecking, Phys. Rev. A **50**, 1435 (1994).

[19] T. Schenkel, M. A. Briere, A. V. Barnes, A. V. Hamza, K. Bethge, H. Schmidt-Böcking, and D. H. Schneider, Phys. Rev. Lett. **79**, 2030 (1997).

[20] M. Hattass, T. Schenkel, A. V. Hamza, A. V. Barnes, M. W. Newman, J. W. McDonald, T. R. Niedermayr, G. A. Machicoane, and D. H. Schneider, Phys. Rev. Lett. **82**, 4795 (1999).

[21] H. Hanafy, M. Bjorkhage, S. Leontin, E. Lindroth, Z. D. Pešić, Gy. Vikor, and R. Schuch, Phys. Scr., T **92**, 47 (2001).

[22] E. Beebe, L. Ljiljeby, A. A. Engstrom, and M. Bjorkhage, Phys. Scr. **47**, 470 (1993).

[23] W. K. Chu, J. W. Meyer, and M. A. Nicolet, *Backscattering Spectroscopy* (Academic Press, New York, 1978).

[24] J. F. Ziegler, SRIM-2000 Instruction Manual, 2000; see also http://www.research.imb.com/ionbeams/home.html\#SRIM

[25] J. P. Biersack and L. G. Haggmark, Nucl. Instrum. Methods **174**, 257 (1980).

[26] R. Schuch, D. Schneider, D. A. Knapp, D. DeWitt, J. McDonald, M. H. Chen, M. W. Clark, and R. E. Marrs, Phys. Rev. Lett. **70**, 1073 (1993).

[27] G. A. Machicoane, T. Schenkel, T. R. Niedermayr, M. W. Newmann, A. V. Hamza, A. V. Barnes, J. W. McDonald, J. A. Tanis, and D. H. Schneider, Phys. Rev. A **65**, 042903 (2002).

[28] Z. D. Pešić *et al.* (unpublished).

[29] J. Anton, K. Schulze, P. Kurpick, W. D. Sepp, and B. Fricke, Hyperfine Interact. **108**, 89 (1997).
[30] P. Kurpick, W. D. Sepp, and B. Fricke, Phys. Rev. A **51**, 3693 (1995).
[31] R. Díez Muiño, A. Salin, N. Stolterfoht, A. Arnau, and P. M. Echenique, Phys. Rev. A **57**, 1126 (1998).
[32] J. C. Slater, Phys. Rev. **36**, 57 (1930).
[33] W. Bambynek, B. Crasemann, R. W. Fink, H. U. Freund, H. Mark, C. D. Swift, R. E. Price, and P. V. Rao, Rev. Mod. Phys. **46**, 853 (1974).
[34] E. J. McGuire, Phys. Rev. A **6**, 851 (1972); **9**, 1840 (1974).
[35] P. Palmeri, P. Quinet, N. Zitane, and N. Vajck, J. Phys. B **34**, 4125 (2001).
[36] M. H. Chen and B. Crasemann, Phys. Rev. A **30**, 170 (1984).